HEALTH AND MEDICINE

Accelerating thrombolysis using a precision and clot-penetrating drug delivery strategy by nanoparticle-shelled microbubbles

Siyu Wang[1], Xixi Guo[1], Weijun Xiu[1], Yang Liu[2], Lili Ren[1], Huaxin Xiao[1], Fang Yang[2], Yu Gao[1]*, Chenjie Xu[3], Lianhui Wang[1]*

Conventional thrombolytic drugs for vascular blockage such as tissue plasminogen activator (tPA) are challenged by the low bioavailability, off-target side effects and limited penetration in thrombi, leading to delayed recanalization. We hypothesize that these challenges can be addressed with the targeted and controlled delivery of thrombolytic drugs or precision drug delivery. A porous and magnetic microbubble platform is developed to formulate tPA. This system can maintain the tPA activity during circulation, be magnetically guided to the thrombi, and then remotely activated for drug release. The ultrasound stimulation also improves the drug penetration into thrombi. In a mouse model of venous thrombosis, the residual thrombus decreased by 67.5% when compared to conventional injection of tPA. The penetration of tPA by ultrasound was up to several hundred micrometers in thrombi. This strategy not only improves the therapeutic efficacy but also accelerates the lytic rate, enabling it to be promising in time-critical thrombolytic therapy.

INTRODUCTION

Blood vessel occlusion partly or completely blocks the flow of blood in a blood vessel, often resulting in life-threatening diseases such as coronary infarction, ischemic stroke, and pulmonary embolism (*1*–*3*). While infusion of thrombolytic drugs such as tissue plasminogen activator (tPA) through either systematic administration or catheter placement has greatly improved the survival rates and the life quality of the patients, challenges emerge such as the low bioavailability of tPA, poor delivery efficiency, and the resistance of fibrin and platelet-rich thrombi to thrombolytic drugs, resulting in stepwise or slow recanalization (*4*–*7*).

The targeted and controlled delivery of thrombolytic drugs has been proposed to address the challenges, aiming at improving the bioavailability of tPA, targeted delivery, and clot lysis acceleration (*8*–*11*). For example, shear-stress responsive carriers targeting the narrowed or obstructed blood vessels could lower the required doses of tPA and minimize the side effects (*12*). Rotating magnetic nanomotors elevate tPA transport at the interface of blood and clot, resulting in accelerated lytic rate and improved thrombolytic efficacy (*13*). Acoustically trigged release of tPA from tPA-loaded echogenic liposomes enhance the thrombolytic activity due to cavitation or acoustically driven diffusion effects (*14*, *15*). While these advancements are encouraging, they only partially address the above challenges and have not been translated into clinical practice.

There are three keys in this process, i.e., maintenance of drug activity, selected accumulation in the clots, and diffusion/penetration throughout the clot tissue (*16*–*18*). Although shear-activated nanotherapeutics is promising to improve the delivery efficiency specifically to clots, the loaded tPA by surface conjugation tend to be deactivated by the inhibitors in the blood (*12*). Ultrasound can trigger the tPA release from tPA-loaded echogenic liposomes directly to the site of a clot visualized by ultrasound imaging; however, it has been limited because of the lack of targeted strategy (*14*, *15*). The thrombolysis efficacy of these methods was also challenged by the limited clot penetration of released tPA. Magnetically targeted delivery of tPA and rotating enhanced mass transfer (diffusion) of tPA have been achieved by magnetic porous micromotors (*19*). This method addressed the challenges mentioned above and improved the therapeutic efficacy of blood clot in the mice middle cerebral, thereby representing a potential solution for accelerating thrombolysis. Despite promising, a trigger of the release of tPA from carriers will reduce the unwanted leakage during circulation. Meanwhile, facilitating the penetration of tPA rapidly during the treatment will initiate the enlarged interaction area between tPA and clots, probably further improving the thrombolysis efficacy.

To address this unmet need, we propose a precision delivery strategy using the magnetic targeting and ultrasound-triggered release. Specifically, this strategy uses a multifunctional nanosystem with responsiveness to the magnetic field and ultrasound by synergizing different functions of its components (Fig. 1A). This system stably maintains the tPA activity during circulation. When guided by a magnet, it directly targets to the thrombi and then is remotely activated for drug release using low-intensity ultrasound. The ultrasound stimulation also rapidly improves drug penetration into thrombi tissue within several minutes.

As a proof of concept, we have developed a nanoparticle-shelled microbubble (MMB-SiO_2-tPA) for the targeted delivery of tPA to clots. The microbubbles were made through nanoparticle self-assembly at the liquid-air interface (Fig. 1B). The prepared microbubbles have a layer of nanoparticles that are densely packed around the air core, sealing the air and preventing the release of loaded tPA in circulation. The magnetic component of the shell facilitates the targeting of the microbubbles to clots under a magnetic field. Upon ultrasound stimulation, microbubbles oscillate, and shelled nanoparticles are

[1]Key Laboratory for Organic Electronics and Information Displays and Jiangsu Key Laboratory for Biosensors, Institute of Advanced Materials (IAM), Jiangsu National Synergistic Innovation Center for Advanced Materials (SICAM), Nanjing University of Posts and Telecommunications, Nanjing 210023, China. [2]State Key Laboratory of Bioelectronics, Jiangsu Key Laboratory for Biomaterials and Devices, School of Biological Science and Medical Engineering, Southeast University, Nanjing 210096, China. [3]School of Chemical and Biomedical Engineering, Nanyang Technological University, 70 Nanyang Drive, Singapore 637457, Singapore.
*Corresponding author. Email: iamygao@njupt.edu.cn (Y.G.); iamlhwang@njupt.edu.cn (L.W.)

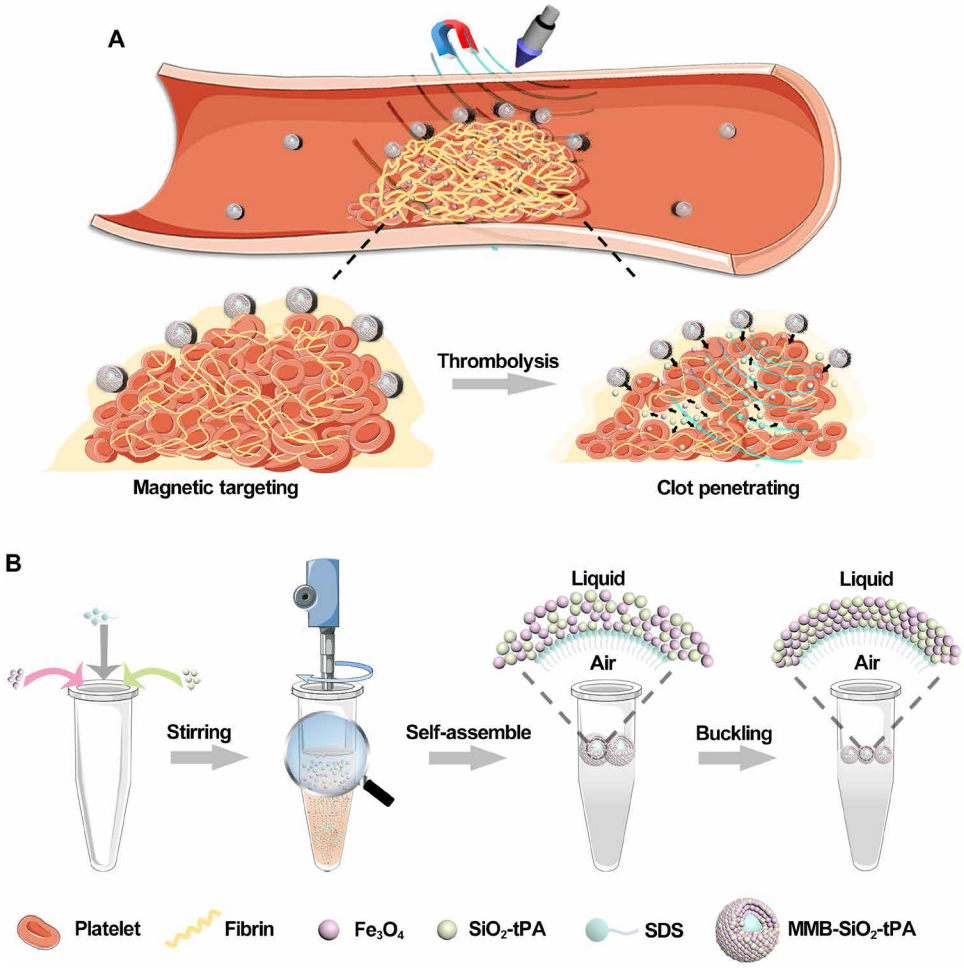

Fig. 1. Precision delivery strategy using the magnetic targeting and ultrasound-triggered release. (**A**) Illustration of targeted delivery and controlled release for thrombolysis. (**B**) Illustration of the synthesis of nanomedicine-shelled microbubble (i.e., MMB-SiO_2-tPA).

released from the bubbles following the microstreaming. The momentum received from the oscillation allows the nanoparticles to penetrate into the agarose-fibrin gel and femoral vein clots up to 1 cm and hundred micrometers, respectively. The penetrated tPA accelerates the mass transfer into the interior of the clots, thereby improving the lytic rate and thrombolysis efficacy.

RESULTS

Preparation and characterization of nanoparticle-shelled microbubbles

Nanoparticle-shelled microbubbles (MMB-SiO_2-tPA) are composed of a gas core and a shell of nanoparticles. The core is air, while the nanoparticles are a mixture of magnetic iron oxide nanoparticles (50 nm; MMB) and tPA-containing mesoporous silica nanoparticles (50 nm; SiO_2-tPA). Under the presence of anionic surfactant (e.g., SDS) and agitation, gas is encapsulated within the surfactant, and nanoparticles assemble at the air-liquid interface. Their size can be precisely controlled by adjusting the agitation speed and the concentration of nanoparticles (*20*).

The structure and morphology of prepared MMB-SiO_2-tPA were shown in Fig. 2A. The mean thickness of the nanoparticle shells was around 1.5 μm, accounting for approximately 20 to 30 layers of assembled nanoparticles (fig. S1). Elemental mapping confirmed the presence of Fe, Si, and O on the shell of the MMB-SiO_2-tPA with homogeneous distribution (Fig. 2B). The microbubbles were compacted with spherical shape and had a mean diameter of 5.36 ± 1.44 μm (Fig. 2C), similar to the microbubbles used in clinics (2 to 8 μm usually) (*21*). To identify whether the mesoporous silica nanoparticles were loaded in the microbubble shell, SiO_2-tPA nanoparticles were replaced with SiO_2-Cy5.5 nanoparticles. In a confocal image, red fluorescence surrounded the shell of most microbubbles, while no fluorescence was found in the air core, suggesting the structure of nanoparticle-shelled microbubble and the efficient assembly of silica nanoparticles (fig. S2). Being out of the focal plane resulted in centered fluorescence and smaller sizes of the microbubbles in the same confocal image. Quantitative element analysis by inductively coupled plasma optical emission spectrometry (ICP-OES) revealed the contents of Fe and Si in MMB-SiO_2-tPA samples (Fig. 2D), and the content of tPA was quantified by bicinchoninic acid (BCA) assay (Fig. 2E). After the number of MMB-SiO_2-tPA in different volume of solutions was counted (Fig. 2F), the amounts of Fe, Si, and tPA were determined as 1.25×10^{-8}, 2.99×10^{-10}, and 6.63×10^{-12} g per MMB-SiO_2-tPA, respectively. The encapsulation efficiency of tPA was 47.9%.

tPA has a relatively short half-life (about 2 to 6 min) in circulation as there are inhibitors such as plasminogen activator inhibitor–1 (PAI-1; the major inhibitor of tPA) (*22*). When it was loaded in the

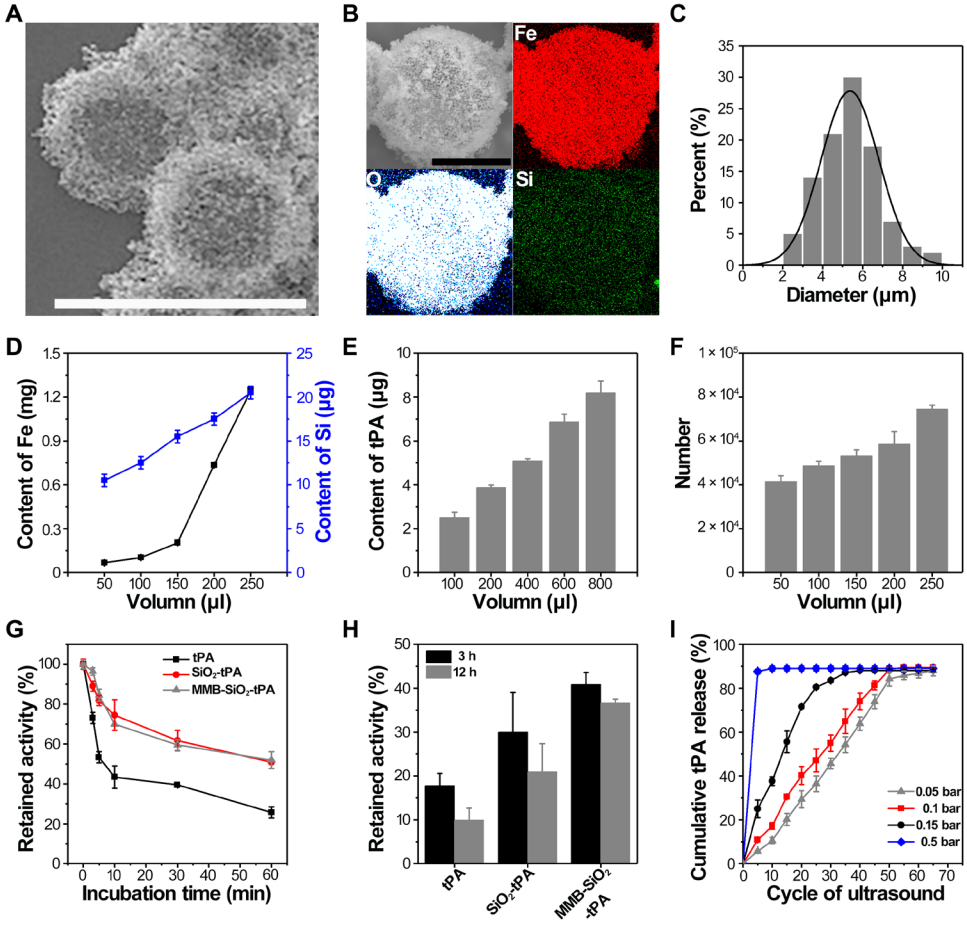

Fig. 2. Preparation, characterization, tPA activity maintenance of MMB-SiO_2-tPA, and controlled tPA release. (**A**) Environmental scanning electron microscope image of MMB-SiO_2-tPA in bright field mode. Scale bar, 10 μm. (**B**) Scanning electron microscopy and elemental mapping of a single MMB-SiO_2-tPA. Scale bar, 5 μm. (**C**) The diameter distribution of the MMB-SiO_2-tPA; $n = 200$. (**D**) Contents of iron and silicon in different volumes of MMB-SiO_2-tPA quantified by ICP-OES. (**E**) Content of thrombolytic drug (tPA) in different volumes of MMB-SiO_2-tPA by BCA assay. (**F**) Counting MMB-SiO_2-tPA in different volumes of solutions. (**G**) In vitro enzymatic activity of native tPA, SiO_2-tPA, and MMB-SiO_2-tPA versus time in the presence of plasminogen activator inhibitor-1 (PAI-1). (**H**) The retained activity of tPA after 3 and 12 hours in the presence of PAI-1. (**I**) Cumulative release profiles of thrombolytic drug tPA from MMB-SiO_2-tPA at different acoustic pressure of ultrasound. Error bars in all figures indicated the standard divisions by at least triplicate experiments.

mesoporous silica nanoparticles, its stability can be substantially improved. For example, we compared the availability of tPA under the presence of the PAI-1 for three formulations (i.e., native tPA, SiO_2-tPA, and MMB-SiO_2-tPA). The activity of tPA in all groups decreased with time when exposed to PAI-1 (Fig. 2G). The retained activity of native tPA decreased to 25% when exposed to PAI-1 for 60 min, while more than 50% of tPA in both SiO_2-tPA and MMB-SiO_2-tPA maintained their activity at the same time. After 12 hours of incubation with PAI-1, MMB-SiO_2-tPA still maintained 36% of the tPA activity, which was higher than 16 and 8% obtained by SiO_2-tPA and native tPA, respectively (Fig. 2H). It is worth noting that the close packing of shelled nanoparticles on the microbubble surface prevented the release of tPA from silica nanocarriers without an ultrasound trigger, resulting in the higher retained activity of MMB-SiO_2-tPA than that of SiO_2-tPA.

Controlled release of tPA from MMB-SiO_2-tPA under stable oscillations

This microbubble-based drug delivery system is expected to release the drug upon the ultrasound stimulation. Traditionally, most microbubbles are stabilized by a "rigid" shell formed by polymer, silica, or protein (*21*, *23*). The release of cargos depends on the bubble inertial expansion and explosion, a phenomenon called "cavitation" that usually requires high acoustic-driven force (i.e., high-intensity ultrasound) (*24*). To reduce the risk of tissue injury in cavitation, drug release by stable microbubble oscillations (fig. S3) that activated by low-intensity ultrasound is an alternative (*20*, *25*, *26*).

We compared tPA release under both microbubble stable oscillations and cavitation. Stable oscillation was achieved when the ultrasound intensity was set below the threshold of activating microbubble cavitation (0.4 bar or 0.04 MPa in our experiment) (*20*). Shelled nanoparticles are then released by these microbubble oscillations accompanied by the microstreaming. For example, approximately 5% of tPA were released when ultrasound was applied for five cycles with the acoustic pressure of 0.05 bar (i.e., 0.005 MPa; Fig. 2I). If the ultrasound was kept on applying for another 60 cycles, then the amount of released tPA reached a plateau to around 90%. Owing to the stable oscillations of MMB-SiO_2-tPA that without microbubble collapse, a stepwise release of tPA was achieved with increasing the number of cycles of applied ultrasound. When most nanoparticles

were released, MMB-SiO_2-tPA gradually dissolved in solution. By increasing the acoustic pressure to 0.1 and 0.15 bar, more rapid release kinetics were observed compared to that by 0.05 bar, suggesting that more intense oscillations happened. If the acoustic pressure (i.e., 0.5 bar or 0.05 MPa) was higher than the cavitation threshold, then almost 90% of tPA were released at the first five cycles of ultrasound due to the bubble collapse by the cavitation effect. On the basis of these findings, on-demand release of tPA can only be achieved by stable microbubble oscillations under low-intensity ultrasound.

Magnetically guided targeting of MMB-SiO_2-tPA on the clots

We first validated the response of MMB-SiO_2-tPA toward the magnetic guidance in an in vitro vessel system. The MMB-SiO_2-tPA were dissolved in cell culture medium and pumped by a syringe into a polyethylene vessel (diameter of 3 mm) with a speed (1.2 cm s^{-1}) that mimics the blood flow. When a magnet was placed adjacent to the vessel, MMB-SiO_2-tPA accumulated to the magnet in approximately 2 s (fig. S4). Once the magnet was removed, the accumulated MMB-SiO_2-tPA swiftly dispersed and circulated with the liquid flow without noticeable attachment to the vessel wall.

Next was to confirm this magnetically guided targeting in vivo. Ultrasound imaging was used to track this process, as the microbubbles can enhance the contrast in ultrasound imaging. As shown in Fig. 3B, the B mode acoustic intensity of a phantom was enhanced by three times after injection of MMB-SiO_2-tPA into the phantom. The enhancement of contrast mode was much more significant, which is increased by 17 times after injection (Fig. 3D).

The animal model was built on mice through ferric chloride infiltration of the femoral vein. We imaged the mice before and after the intravenous injection with MMB-SiO_2-tPA. A magnet was placed adjacent to the thrombi for magnetic targeting (Fig. 3A). The acoustic intensities of both B mode and contrast mode of the thrombi in the femoral vein were slightly increased after intravenous injection of MMB-SiO_2-tPA for 5 min, which might be attributed to the presence of small amounts of MMB-SiO_2-tPA at the thrombi lesion through blood circulation (Fig. 3C). Once a magnet was applied, significant enhancement of the acoustic intensities of both B mode and contrast mode was observed (increased by 1.4 and 2.6 times, respectively), suggesting the accumulation of MMB-SiO_2-tPA at the thrombi site by magnetic targeting (Fig. 3E). Therefore, MMB-SiO_2-tPA can be magnetically guided to the thrombi and used as ultrasound contrast agents for thrombi diagnosis, simultaneously monitoring the delivery efficiency of therapeutic agents noninvasively.

Low-intensity ultrasound enhances tPA penetration and accelerates thrombolysis in a gel assay

In the fibrinolysis process, tPA activates plasminogen and converts it into plasmin, which is able to cleave fibrin into a soluble product (*27*). To validate the effectiveness of fibrin lysis and the penetration of tPA in three dimensions, a vertical-channel gel system composed of fibrinogen, thrombin, plasminogen, and agarose was developed. Fibrin formed by the reaction of fibrinogen and thrombin were dispersed within the agarose gel with good homogeneity and appeared pale white throughout the gel (Fig. 4A, top left). Once fibrin interacted

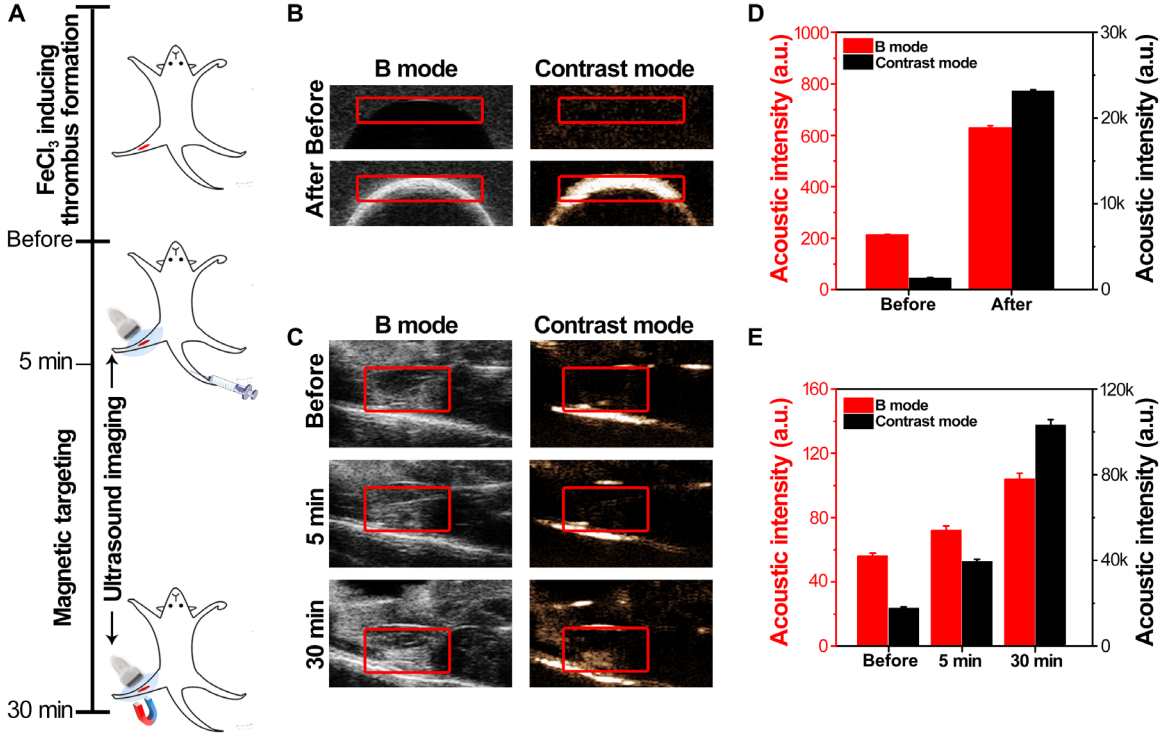

Fig. 3. Ultrasound imaging of thrombi after intravenous injection of MMB-SiO_2-tPA in a femoral vein thrombi–bearing mouse model. (**A**) Schematic illustration of the ultrasound imaging and magnetic targeting process in a femoral vein thrombosis model. (**B**) In vitro ultrasound phantom images of MMB-SiO_2-tPA in B mode and contrast mode. (**C**) In vivo ultrasound images of femoral vein thrombi before and after MMB-SiO_2-tPA injection in B mode and contrast mode. A magnet was placed adjacent to the femoral vein after 5 min after MMB-SiO_2-tPA injection. (**D**) The acoustic intensities of the interested area (red frame) quantified in ultrasound phantom images. a.u., arbitrary units. (**E**) The acoustic intensities of the interested area (red frame) quantified in ultrasound images of the mouse model. Error bars in all figures indicated the standard divisions by at least triplicate experiments.

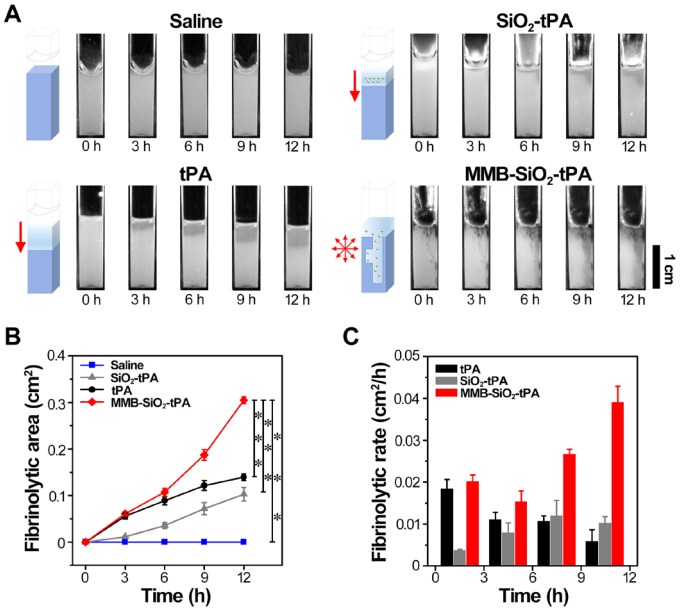

Fig. 4. In vitro fibrin-lysis assay by a vertical-channel gel system composed of agarose-fibrin. (**A**) Schematic diagrams and representative photographs of the fibrinolytic process of the agarose-fibrin gel incubated with saline, native tPA, SiO_2-tPA, and MMB-SiO_2-tPA at different thrombolysis times, respectively. (**B**) Quantification of fibrinolytic area of fibrin over time incubated with saline, native tPA, SiO_2-tPA, and MMB-SiO_2-tPA ($n = 5$; ***$P < 0.001$). (**C**) The mean fibrinolytic rate of fibrin at different time intervals incubated with native tPA, SiO_2-tPA, and MMB-SiO_2-tPA ($n = 5$).

with tPA, degraded products will make the gel transparent (dark area), indicating the lysis area by tPA. As shown in Fig. 4, following the addition of tPA from the top of the vertical channel, a stepwise enlargement of the lysis area with time is presented from the top of the gel (Fig. 4A, bottom left). The stepwise lysis by tPA, the standard thrombolysis process in clinics, was attributed to the mass transfer dynamics of tPA at the liquid-gel (or liquid-thrombi) interface, suggesting limited penetration of tPA in the gel. A similar finding was also found in the group treated by SiO_2-tPA (Fig. 4A, top right), where retarded lysis compared to native tPA was observed because of the delayed release of tPA from SiO_2 nanocarriers (fig. S5). To facilitate the penetration of SiO_2-tPA into the gel, MMB-SiO_2-tPA (equivalent amount of tPA with the groups of native tPA or SiO_2-tPA) were concentrated at the liquid-gel interface by a magnet and then irrigated by low-intensity ultrasound (0.2 bar, i.e., 0.02 MPa) for stable oscillations. The penetration of both iron oxide and silica nanoparticles throughout the gel was observed immediately once the stable oscillations happened, where black dots appeared deep inside the gel along the vertical channel (Fig. 4A, bottom right). The enlargements of dark areas at multiple locations indicated that the lysis happened not only at the liquid-gel interface but also around the nanocarriers that penetrating into the gel. Consequently, the fibrinolytic efficacy (quantified by fibrinolytic areas; Fig. 4B) of MMB-SiO_2-tPA was higher than native tPA after 6-hour treatment. The mean fibrinolytic rate obtained by MMB-SiO_2-tPA markedly increased during the period from 6 to 12 hours after treatment (Fig. 4C). However, the fibrinolytic rate obtained by native tPA decreased with time because of the consumption or degradation of tPA. It is worth noting that these improvements of both fibrinolytic efficacy and fibrinolytic rate by MMB-SiO_2-tPA compared to native tPA were achieved in a confinement space without blood flow. Considering the blood flow in vivo that resulted in fast clearance of tPA, the improvement of tPA penetration will retain the delivered tPA within the clots and, lastly, accelerate thrombolysis and improve the efficacy of tPA treatment.

Low-intensity ultrasound improves thrombolysis efficacy in ex vivo blood clots

The thrombolysis efficacy was further evaluated in the ex vivo blood clots, which were prepared by fresh mice blood and thrombin (Fig. 5A). With dissolution, the clots in tubes shrank, and the supernatants became red. As expected, clots treated by saline barely lysed in a period of 12 hours, suggesting the stability of prepared clots. When clots were treated with native tPA, SiO_2-tPA, or MMB-SiO_2-tPA, all clots lysed stepwise into smaller sizes, while the supernatants gradually changed from colorless into blood red (Fig. 5B). The black color presented in MMB-SiO_2-tPA–treated group was generated by the released iron oxide nanoparticles. The dissolution efficiencies were quantified by measuring the mass loss of the clots at 3 and 12 hours after treatments. During the first 3 hours (Fig. 5C), clots treated by MMB-SiO_2-tPA exhibited similar dissolution efficiency (approximately 32%) to those by native tPA (approximately 27%), which was higher than those obtained by SiO_2-tPA or saline treatments (17 and 7%, respectively). After 12 hours (Fig. 5D), MMB-SiO_2-tPA treatment achieved the highest dissolution efficiency, which was approximately 93%, compared to those obtained by native tPA, SiO_2-tPA, or saline treatments (68, 51, and 16%, respectively). The amounts of hemoglobin (released during clot lysis) in the supernatants at 12 hours after treatments exhibited similar trends to the dissolution efficiencies, confirming the results obtained in the ex vivo experiments. As this experiment was performed in a static situation without blood flow, the improvement of dissolution efficiency in the MMB-SiO_2-tPA–treated group might be attributed to the enhanced penetration and retained activity of tPA.

Low-intensity ultrasound improves the efficacy of femoral vein thrombolysis in a mouse model

To investigate whether the clot-penetrating strategy was applicable to in vivo animal models, we performed different treatments to the femoral vein thrombi of a mouse model. Male C57/BL6J mice were pretreated with $FeCl_3$ for infiltration to form the clots, then were injected with MMB-SiO_2-tPA through the tail vein, and were treated with magnetic targeting and the low-intensity ultrasound in sequence (Fig. 6A). Control groups included mice injected with saline, native tPA, and SiO_2-tPA, respectively. The images of the thrombi were recorded every 3 hours before the mice were sacrificed at 12 hours after treatments. As shown in Fig. 6B, the femoral vein exhibited dark areas where $FeCl_3$ filter paper was placed, indicating the successful formation of the blood clots. The dark areas of the femoral vein treated by saline became longer with time, suggesting the progression of venous thrombosis. When native tPA were intravenously injected, the dark areas shrank in size and became shallow, indicating that clot lysis happened gradually with time. By this dosage of native tPA (100 μl, 10 μg ml^{-1}), the blocked veins were not thoroughly recanalized, as shallow shadows still presented at 3 and 12 hours after treatment. Although SiO_2-tPA holds the ability to protect native tPA against its inhibitors in blood, SiO_2-tPA treatment only achieved similar thrombolysis efficacy to that of native tPA

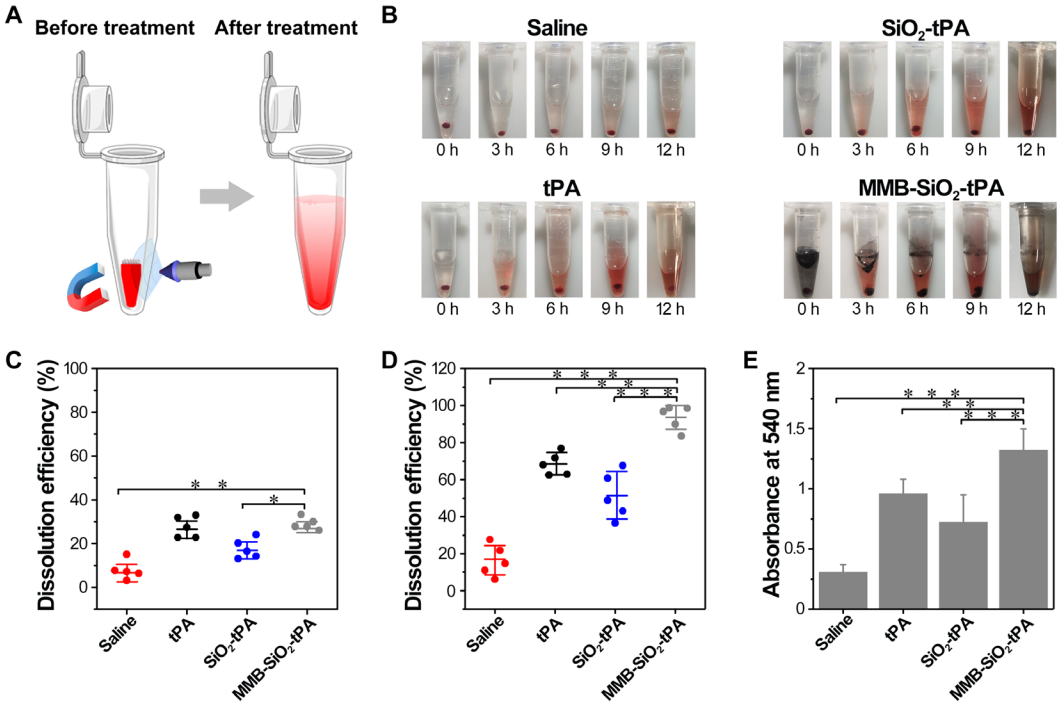

Fig. 5. Assessment of dissolution efficiency in ex vivo blood clots. (**A**) Schematic illustration of the blood clot dissolution treatment process under the magnetic field combined with low-intensity ultrasound. (**B**) Representative images of the thrombolysis processes at 0, 3, 6, 9, and 12 hours after being treated by saline, native tPA, SiO_2-tPA, and MMB-SiO_2-tPA, respectively. (**C**) Quantification of the dissolution efficiency by measuring the mass loss of the blood clot at 3 hours after treatments. (**D**) Quantification of the dissolution efficiency by measuring the mass loss of the blood clot at 12 hours after treatments. (**E**) Absorbance values ($\lambda = 540$ nm) of the supernatants at 12 hours after treatments; $n = 5$; $^*P < 0.05$, $^{**}P < 0.01$, and $^{***}P < 0.001$.

treatment, suggesting the low delivery efficiency of SiO_2-tPA to clots. With the equivalent amount of tPA, the dark areas of MMB-SiO_2-tPA–treated veins faded completely even at 3 hours after treatment. The histological results (Fig. 6C) of the femoral veins were in good agreement with the results in Fig. 6B. Ideally, the thrombus is considered to be a cylinder, and the quantification of the volume of the clots reveals the thrombolysis efficacy. Alternatively, quantification of the thrombus area (% vein lumen) by measuring the cross-sectional areas of the clots and the veins in the histological images provides a rough estimate of the thrombosis area (*28*). Still, MMB-SiO_2-tPA treatment achieved the optimal thrombolysis efficacy, resulting in the least thrombus area (approximately 13%), whereas the percentages were 66, 40, and 50% for treatments with saline, native tPA, or SiO_2-tPA, respectively (Fig. 6D). It is worth noting that, according to the histological analysis (Fig. 6C and fig. S7), two of four femoral veins treated by MMB-SiO_2-tPA achieved complete recanalization. Furthermore, the improved penetration of released nanoparticles was evidenced by the histological images of the clots (Fig. 6E). The shelled nanoparticles (black dots) mainly attached to the periphery of the clots without an ultrasound trigger. When triggered by low-intensity ultrasound, shelled nanoparticles were released and penetrated into the interior of the clots, resulting in a relatively homogenous distribution of nanoparticles within the clots.

Safety assessment of the precision delivery strategy

To evaluate the safety of the precision delivery strategy in vivo, MMB-SiO_2-tPA were intravenously administrated to the mice, and the major organs were collected. As shown in the histological images (fig. S8A), no obvious organ damage or inflammatory lesion appeared in both short-term (i.e., 1 day) and long-term (i.e., 7 days) periods. Meanwhile, serum biochemistry assay and complete blood panel tests were studied by comparison between healthy mice and MMB-SiO_2-tPA–injected mice (after 7 days) (fig. S9). The results showed no significant differences in all measurement indicators between the two groups, suggesting the good biocompatibility of MMB-SiO_2-tPA. The SiO_2 nanoparticles were mainly accumulated in the liver and kidney after 24 hours after injection, while the distribution mainly in the spleen was observed for iron oxide nanoparticles (fig. S10). The biodistribution of MMB-SiO_2-tPA in mice suggested their clearance by the reticuloendothelial system.

In addition, the thrombolytic drug always results in bleeding complications because of the off-target action. For example, the circulating tPA breaks down the fibrinogen in the blood, leading to abnormal hemostatic and hemorrhagic side effects (*29*). To evaluate the influence on hemostasis of the MMB-SiO_2-tPA, tail bleeding time was tested on a mouse model. Mice were first intravenously injected with saline, native tPA, or MMB-SiO_2-tPA (with the equivalent amount of tPA), respectively, and then their tails were cut by a scalpel (fig. S8B). The tail bleeding time of mice treated with native tPA (approximately 7.6 min) was almost fourfold as much as that of saline-treated group (approximately 1.8 min), indicating the significant abnormal hemostatic side effect. In contrast, the administration of MMB-SiO_2-tPA without an ultrasound trigger presented a similar bleeding time (approximately 2.2 min) to the saline group, suggesting the limited off-target action and bleeding complication.

Last, but not the least, the safety assessment of ultrasound intensity on mice vascular injury was performed. The applied high-intensity ultrasound (above 0.04 MPa, i.e., 0.4 bar) used to activate cavitation

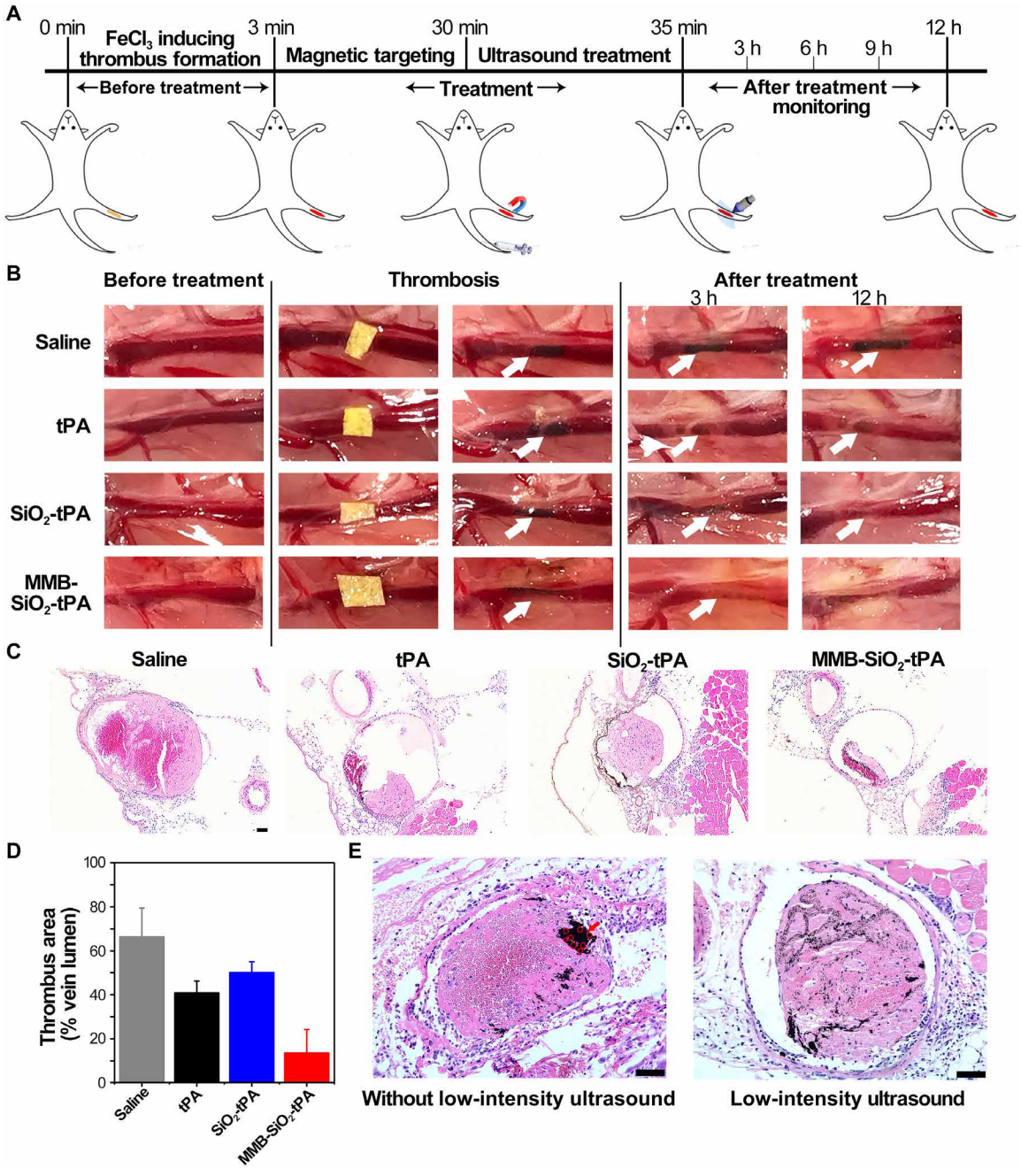

Fig. 6. Low-intensity ultrasound improves the efficacy of femoral vein thrombolysis in a mouse model. (**A**) Schematic illustration of the treatment procedures of a femoral vein thrombosis mouse model. (**B**) Representative images of thrombolysis evaluation after treatment with saline, native tPA, SiO_2-tPA, and MMB-SiO_2-tPA, respectively. The white arrows indicate the inducted thrombi ($n = 4$). (**C**) Representative histological analysis of the femoral vein after treatment with saline, native tPA, SiO_2-tPA, and MMB-SiO_2-tPA for 12 hours, respectively ($n = 4$). Scale bar, 50 μm. (**D**) Quantification of the thrombus area (% vein lumen) in femoral vein in different treatment groups ($n = 4$). (**E**) Representative histological analysis of the femoral vein after administration and magnetic targeting of MMB-SiO_2-tPA with or without low-intensity ultrasound. The red arrow indicates the enrichment of MMB-SiO_2-tPA, and the red circles indicate the MMB-SiO_2-tPA with an intact structure. Scale bars, 50 μm.

might cause endothelial injury and intracerebral hemorrhage (in treatment of stroke), which raised safety issues (*30*–*32*). MMB-SiO_2-tPA were intravenously injected into the mice and targeted to the tail vein, followed by ultrasound treatment with the intensity to trigger bubble cavitation (0.5 bar) and stable oscillations (0.2 bar), respectively. As shown in fig. S8C, deformation of the vascular wall treated by high-intensity ultrasound was observed because of the bubble cavitation effect. The vascular wall became wrinkled and thinner or even ruptured at the thinnest locations (the black arrow in fig. S8C). In contrast, as the ultrasound intensity decreased by more than a half, the vascular wall remained intact with no deformation of the structure. Thus, the precision delivery strategy by

low-intensity ultrasound exhibited satisfactory safety with limited bleeding complication and vascular injury.

DISCUSSION

This work proposed a precision delivery strategy to achieve the targeted and controlled delivery of thrombolytic drugs for thrombolysis. There are three criteria that must be met in this process, i.e., activity maintenance in circulation, targeting to clots, and penetration into clots.

To keep the activity of drugs in circulation, we first loaded tPA into mesoporous silica nanoparticles, which protect the activity of tPA against its inhibitors in the blood. Besides, the stability of nanomedicine in circulation is also important for the activity maintenance and the bioavailability of tPA. In our design, nanoparticles with different functions were integrated into an ultrasound-responsive microbubble through self-assembly and stabilized by the "buckling effect." Specifically, when a strong shear flow is created during agitation of the mixture solution, microbubbles first form because of air entrainment and fragmentation. Because of the hydrophobic surface property, the nanoparticles self-assemble on the microbubble interfaces. When the resultant solution was stored in the ambient, the microbubbles shrink because of gas diffusion, while the nanoparticles remain attached to the interfaces. Until the bubble size reduces to sufficiently small for close packing, the nanoparticles buckle (Fig. 1B). On one hand, this buckling resists the bubble surface area reduction; on the other hand, the multilayered packing also shields the gas diffusion from the gas core. Eventually, these microbubbles reach an equilibrium size with a multilayered nanoparticle shell resulting in superior stability. The close packing of nanoparticles also prevents the release of loaded tPA to the blood, decreasing the contact possibility between tPA and its inhibitors. Comparing to the delivery strategy using surface conjugation of tPA or noncontrolled release of tPA, this strategy can improve the delivery efficiency of active tPA to the clots (*12*, *19*). The activity of tPA is maintained with a half-life of 1 hour in the presence of its inhibitors in vitro (Fig. 2H), which is much longer than that of native tPA (approximately 5 min). The stability of MMB-SiO_2-tPA in circulation was evidenced by the US imaging in a mouse model, where enhanced contrast was observed in the blood vessel even after 30 min after injection. Thereby, the precision delivery strategy meets the first criteria in the thrombolysis process of a nanomedicine, i.e., maintained the activity of tPA in blood circulation.

Targeted delivery improves delivery efficiency and specificity, thus reduces the required dose and side effects. Targeting strategies using RGD (Arg-Gly-Asp) motif (binding to active platelet integrin GPIIb/IIIa) or anti-fibrin antibody are still challenged by the relatively low targeting efficiency due to the protein corona of the nanomedicine formed in the blood and the heterogeneity of different clots from individuals (*33*–*35*). For example, there was no significant difference in the recanalization rate of the rabbit aorta thrombus model by injection of tPA-loaded echogenic liposomes with or without ultrasound treatment (*15*). The ultrasound was speculated to potentiate the catalytic activity of exposed liposome-associated tPA, rather than cause the release of the enzyme into the clots. The improvement of the thrombolysis efficacy might be compromised by the poor delivery efficiency without targeting strategy and the limited penetration of tPA within the clots. Magnetically targeted delivery of tPA to the blood clot in mouse middle cerebral artery has been achieved in the reported work by porous magnetic microrods as carriers (*19*). In our strategy, magnetic targeting can be simply applied to the adjacent tissue of the thrombi diagnosed by ultrasound imaging (Fig. 3E), enabling it to meet the second criteria and to be promising and clinically feasible.

There is limited clot-penetrating strategy that have been reported because of the structure of thrombi, consisting of abundant platelet and well-organized fibrin. Rotating magnetic microrods might generate mechanical force to the cross-linked fibrin, disrupting the structure of the clots and facilitating the penetration of released tPA (*19*). Blood flow of a cerebral artery occlusion mouse model was restored in 25 min by tPA-loaded microrods [tPA (0.13 mg kg^{-1})], which is faster than 85 min required by tPA only with high concentration [tPA (10 mg kg^{-1})]. The significant improvement of the lytic rate and the much less required dosage of tPA were attributed partially to the increased release rate and improved mass transport of tPA and partially to the disruption of the fibrin network by mechanical rotation force leading to the improved penentration of tPA (*19*). In the present work, we aim to show the direct evidence of enhanced penetration of tPA nanocarrier within the clot tissue by low-intensity ultrasound. Previously, we have demonstrated improved tissue penetration of nanoparticles by stable microbubble oscillations (*20*). Briefly, self-assembled nanoparticles form an "elastic shell" due to the weak hydrophobic interaction between nanoparticles. When activated by their resonance frequency with the ultrasound intensity below the threshold of cavitation, microbubbles undergo stable oscillations. As illustrated in fig. S3, under high acoustic pressure, a microbubble shrinks in size, while its shelled nanoparticles are densely packed. Whereas under low acoustic pressure, the microbubble swells, and its shelled nanoparticles are loosely packed, accompanying by the nanoparticles shedding at the outermost layer. Subsequently, the loosely packed nanoparticles reassembled to form the buckled shell when the acoustic pressure increases again. This reassembling of shelled nanoparticles was recorded by a charge-coupled device camera in supplementary movie. The movements of fluorescent silica nanoparticles in the shell revealed the nanoparticle reassembling process during stable microbubble oscillations. It is worth noting that silica nanoparticles were released and moved along with the microstreaming induced by the stable oscillations, suggesting the possibility of penetration improvement in tissues. The penetration of released nanoparticles can be up to 1 cm in the agarose-fibrin gel (Fig. 4A). According to literature (*13*), the lysis process can be described as follows

$$S + T \xrightarrow{K_T} \mathrm{ST(SP)} \xrightarrow{K_P} S + P$$

where S, T, ST, SP, and P is the exposed lysine site, the tPA molecule, tPA-lysine complex, tPA-product complex, and the product, respectively, K_T and K_P are the tPA absorption rate and product desorption rate, respectively. Assuming that the transport-facilitated tPA binding is the rate-limiting step at $C_{\mathrm{tPA}} = 10\ \mu g\ ml^{-1}$ ($K_T << K_P$), then the thrombolysis rate $v = K_T[S][T]$. In all the experiment groups, K_T can be assumed to be a constant. For tPA group, the v decreased with time, which was the result of the decrease of $[T]$ due to the consumption of tPA molecules. According to the release profile of SiO_2-tPA, the initial $[T]$ of SiO_2-tPA group is smaller than that of tPA group, which results in slower thrombolysis rates of SiO_2-tPA (0 to 6 hours) than those of tPA. As SiO_2-tPA continuously replenish the tPA to the surrounding medium, the $[T]$ of SiO_2-tPA (depends on the release and consumption kinetics) might be not

change as significant as that of tPA. Thus, the values of v in SiO_2-tPA group were observed at similar level after 3 hours. For MMB-SiO_2-tPA group, the magnet concentrated the microbubbles (together with the SiO_2-tPA) at the interface of the gel, and then stable microbubble oscillation (by ultrasound for 3 min) released the nanoparticles and facilitated the penetration of SiO_2-tPA into the gel, resulting in increased number of exposed lysine site (i.e., [S]) from the interior of the gel. Considering the smaller [T] of MMB-SiO_2-tPA (the same with SiO_2-tPA) than that of tPA, the observed v of both MMB-SiO_2-tPA and tPA are similar in 0 to 3 hours. The penetration effect on the thrombolysis rate is more prominent for MMB-SiO_2-tPA after 6 hours due to the different changes of [T] for MMB-SiO_2-tPA and tPA groups. Notably, the improved penetration can only be achieved by MMB-SiO_2-tPA under ultrasound. Free tPA and MMB-SiO_2 under ultrasound did not change the lysis speed and manner (from top to the bottom), which are the same with those of tPA group (fig. S6).

In the mouse model, the released nanoparticles can easily reach the center of a venous thrombus with the diameter of 300 μm (Fig. 6E). Thereby, the lysis happened not only at the interface of a clot but also at many interior locations, resulting in accelerated thrombolysis. In a mouse model of venous thrombosis, the residual thrombus decreased by 67.5% when treated with MMB-SiO_2-tPA [tPA (0.03 mg kg^{-1})] compared to conventional injection of tPA [tPA (0.03 mg kg^{-1})]. Note that such a low tPA dosage of MMB-SiO_2-tPA can achieve complete recanalization (two of four femoral veins). The therapeutic efficacy and lytic rate can be further improved by increasing the dosage of loaded tPA for time-critical thrombolytic therapy. The improved penetration of tPA lastly meets the third criteria of the thrombolysis process.

The delivery of the thrombolytic drugs to complex locations such as cerebral embolism, pulmonary embolism, and myocardial infarction is more challenged in comparison to femoral vein thrombus. Although promising results have been shown in both in vitro and in vivo, the present delivery strategy can be further improved for application in embolism at complex locations. First, the size of MMB-SiO_2-tPA can be reduced to avoid fast clearance by the reticuloendothelial system. Last, the circulation time of MMB-SiO_2-tPA is challenged due to its hydrophobic surface property. Cell membrane (e.g., red blood cells and platelets)–coating technology can be applied to prolong the circulation of MMB-SiO_2-tPA, thereby improving the delivery efficiency and therapeutic efficacy (*36*–*39*).

In summary, we conclude that our precision delivery strategy can complete three important steps of nanomedicine for thrombolysis, i.e., activity maintenance in circulation, targeting to clots, and penetration into clots. The accelerated lytic rate and the improved therapeutic efficacy are attributed to the increased effective concentration of tPA at the site of clots, a result by tPA activity maintenance, magnetic targeting, and improved penetration of tPA within the clots. Thus, this strategy holds great promise in thrombi diagnosis and accelerating thrombolysis while reducing the complication risk of tPA and the vascular injury by high-intensity ultrasound.

MATERIALS AND METHODS

Materials

tPA was purchased from Merck (USA). SDS, thrombin from human plasma, plasminogen from human plasma, and the protease substrate H-D-isoleucyl-L-prolyl-L-arginine-p-nitroaniline (S-2288) were purchased from Sigma-Aldrich (USA). Mesoporous silica nanoparticles (SiO_2) were purchased from Shanghai So-Fe Biomedical (China). Fe_3O_4 nanoparticles were purchased from Alfa Aesar (USA). Fibrinogen from human plasma was purchased from Shanghai Yuan Yu Bio-Tech Co. Ltd. (China). Agarose was purchased from BD (USA). All the other chemicals and solvents were purchased from Sigma-Aldrich.

Preparation and characterization of nanomedicine-shelled microbubbles

The nanoparticle-shelled microbubbles were prepared by the previous method (*20*). Briefly, magnetic nanoparticles (Fe_3O_4) were dispersed in deionized water to form a stock solution (10 mg ml^{-1}) and treated with ultrasound for 20 min before use. Next, a mixture solution including 150 μl of SiO_2-tPA nanoparticles (0.2 mg ml^{-1}), 150 μl of SDS (10 mM^{-1}), and 400 μl of Fe_3O_4 nanoparticle (10 mg ml^{-1}) was homogenized at 20,000 rpm for 3 min. After stirring, the nanoparticle-shelled microbubbles were stabilized overnight for close packing of nanoparticles and then purified with deionized water by magnetic separation for three times.

The morphology and the size were observed by a microscope (Olympus IX71, Japan) and an environmental scanning electron microscope (Philips XL30, The Netherlands). The diameters were manually measured from the photos and counted at least for 200 microbubbles. The fluorescent nanoparticle-shelled microbubbles were imaged by the laser scanning confocal microscope (Olympus FV1000MPE, Japan). The content of iron and silicon in different volumes of MMB-SiO_2-tPA was measured by ICP-OES (PerkinElmer, USA). The content of the tPA loaded in MMB-SiO_2-tPA was tested by the BCA protein assay kit.

MMB-SiO_2-tPA maintain tPA activity and release tPA by stable oscillations

The fibrinolytic activity of the tPA was tested using a chromogenic substrate, S-2288, as previously reported (*40*). The native tPA was added to the microtiter plate containing assay buffer [0.1 M^{-1} of tris-HCl (pH 7.4)] and S-2288 (1.0 mM^{-1}) at 37°C. The fibrinolytic activity was calculated by ΔAbs per min at 405 nm for 30 min of reaction. The inhibition efficiencies of tPA were determined by incubation of the same amount of tPA (10 μg ml^{-1}) and active PAI-1 (0.5 nM^{-1}) in 200 μl of assay buffer in a microplate at 37°C for predetermined periods. Then, the residual activities of tPA were then measured by the method described above.

The release of tPA from MMB-SiO_2-tPA by ultrasound with different intensities was tested in vitro. Briefly, the ultrasound frequencies from 10 to 900 kHz with amplitudes starting from 2 to 20 Vpp (peak-to-peak voltage) were adjusted by a function generator (Keysight, USA), while the powers of ultrasound were adjusted from 0.1 to 10% by an amplifier (T&C, USA). The ultrasound was applied through a homemade focused transducer, and each cycle contained 5 s of duration time with a time interval of 1 s. The output ultrasound intensities at the focus of the transducer were monitored by an oscilloscope (Keysight, USA). After different cycles of ultrasound, the supernatants were collected, and the amounts of released tPA were quantified by the BCA protein assay kit.

Magnetic targeting and ultrasound imaging of MMB-SiO_2-tPA

A gel mold with a hole was used as the ultrasound phantom, and 1 ml of MMB-SiO_2-tPA solution was added. The phantom was imaged by a high-resolution microimaging system (VisualSonics Vevo 2100, Canada) using the transducer at 18 MHz with a static state using

both B mode and contrast mode. The center frequency, intensity power, and contrast gain were set as 18 MHz, 10%, and 35 dB, respectively. The mean video intensity in the regions of interest (ROIs) was analyzed by a ultrasound image software.

For in vivo ultrasound imaging, the femoral veins of male C57/BL6J mice were treated with 20% ferric chloride solution. Then, the mice were anesthetized by 10% chloral hydrate solution and imaged by a ultrasound imaging system. After intravenously injected with 100 μl of MMB-SiO_2-tPA for 5 min, the femoral veins were imaged again, followed by magnet placement. The accumulations of MMB-SiO_2-tPA by magnet were monitored by ultrasound imaging with time. The mean video intensity in ROI was analyzed by a ultrasound image software.

Assessment of tPA penetration and fibrinolytic efficacy in gel

Ten milliliters of agarose solution (0.5%) containing 20 μl of thrombin solution (250 U ml^{-1}) was thoroughly mixed with 1 ml of fibrinogen solution (10 mg ml^{-1}) and 10 μl of plasminogen solution (1 mg ml^{-1}). Subsequently, the mixed solution was uniformly added to a vertical channel and incubated at 37°C for 2 hours to form the fibrin gel. The concentrations of native tPA, SiO_2-tPA, and MMB-SiO_2-tPA used in the in vitro, ex vivo, and in vivo experiments were fixed with the equivalent amount (1 μg) of tPA (native tPA, 100 μl of 10 μg ml^{-1}; SiO_2-tPA, 100 μl of 50 μg ml^{-1}; MMB-SiO_2-tPA, 100 μl of concentrated MMB-SiO_2-tPA with the number of 1.5×10^6 ml^{-1}). Afterward, 100 μl of saline, native tPA, SiO_2-tPA, or MMB-SiO_2-tPA with the equivalent concentration of tPA (10 μg ml^{-1}) was added to the channel at the top of the gel and incubated at 37°C for 3, 6, 9, and 12 hours, respectively. For the MMB-SiO_2-tPA–treated group, a magnet was placed at the bottom of the channel, and ultrasound was applied for 3 min with the intensity of 0.2 bar. Last, the fibrinolytic activity of each sample was evaluated by comparing the dark areas of the gel. Briefly, images were first processed to eliminate background and converted into binary (black and white) images. The area of "black" pixels represents the lysis area, while the area of "white" pixels represents the agarose-fibrin gel. To identify the boundary, a threshold was determined by processing the images of tPA group. Threshold value was adjusted to include all of the black area within the threshold of the selected area. Then, the same threshold value was applied to the processing for all the other images.

Assessment of thrombolysis efficacy in ex vivo blood clots

The blood clots were prepared via the previous protocol (*41*). Male mice of C57/BL6J (8 to 10 weeks old) were anesthetized via isofluoride gas. One hundred microliters of fresh blood was obtained from the orbital vein and distributed in several centrifuge tubes containing 50 U of thrombin solution. The tubes were placed at 37°C for 3 hours and then were moved to 4°C for 3 days.

The prepared blood clots were placed into centrifuge tubes containing 1 ml of saline. Then, saline (100 μl), native tPA, SiO_2-tPA, and MMB-SiO_2-tPA with the equivalent concentration of tPA (10 μg ml^{-1}) were added into the solution and incubated at 37°C, respectively. During the incubation, the lysis process was monitored at predetermined time points. For the MMB-SiO_2-tPA–treated group, a magnet was placed beneath the clots, and ultrasound was applied for 5 min with the intensity of 0.2 bar. The weight of blood clots during the lysis was recorded, and the clot lysis efficiencies were calculated. Besides, the supernatants of all samples after 12 hours were collected and measured at OD_{540} (optical density at 540) (optical absorbance).

Assessment of thrombolysis efficacy in a mouse model

All procedures involving animals were approved by the Institutional Animal Care and Utilization Committee at Nanyang Technological University. Male C57/BL6J mice (6 to 8 weeks old) were obtained from Nanjing Qinglongshan Animal Breeding Field. The femoral vein thrombosis was induced according to the previous protocol. Briefly, mice were anesthetized with 10% chloral hydrate (100 μl) by intraperitoneal injection. The left femoral veins of the mice were exposed with a scalpel and forceps. After exposure, a filter paper infiltrated with 20% ferric chloride solution was placed on the surface of the femoral vein vessel for 1 to 2 min. Then, the filter paper was removed, and the vessel was washed with sterilized phosphate-buffered saline. In the end, the visible femoral vein thrombi were formed.

To study the thrombolysis efficacy in vivo, 100 μl of saline, native tPA, SiO_2-tPA, and MMB-SiO_2-tPA with the equivalent amount of tPA (10 μg ml^{-1}) was intravenously injected (n = 4 for each group). For the MMB-SiO_2-tPA–treated group, a magnet was placed adjacent to the clots for 25 min, and then ultrasound was applied for 5 min with the intensity of 0.2 bar. The thrombolysis processes were monitored by taking photos in the next 12 hours. After being euthanized, the vessel tissues were excised from the mice and collected for histological analysis (n = 4 for each group). Sections were processed and analyzed using the Image J software by an investigator blinded to the treatment. The areas of clots were measured, and thrombolytic efficiency was determined by the area ratio of vascular occlusion to total vasculature.

To evaluate the improvement of nanoparticle penetration in clots in vivo, the femoral vein thrombi–bearing mice were divided into two groups (n = 3 for each group). One hundred microliters of MMB-SiO_2-tPA was administrated by intravenous injection, and a magnet was placed adjacent to the thrombi for 25 min. Subsequently, the two groups were treated with or without low-intensity ultrasound (0.2 bar), respectively. After being sacrificed, the vessel tissues were excised from the mice and collected for histological analysis.

Safety assessment of the clot-penetrating strategy

Male C57/BL6J mice (6 to 8 weeks old) were intravenously injected with 100 μl of MMB-SiO_2-tPA. Then, the mice were euthanized after 1 or 7 days, and the main organs were collected for histological analysis. Healthy mice intravenously injected with saline were selected as control group (n = 3 for each group).

Tail bleeding assay was performed via previous methods (*29*). Male C57/BL6J mice were anesthetized with 10% chloral hydrate by intraperitoneal injection. Subsequently, 100 μl of saline, native tPA, and MMB-SiO_2-tPA at the equivalent concentration of tPA (10 μg ml^{-1}) was administered (n = 3 for each group). After 5 min, 1 cm of the distal tail was removed from the mice using a scalpel. The time for hemostasis (bleeding fully stopped for at least 1 min) was recorded.

To investigate the vascular injury by ultrasound, male C57/BL6J mice were anesthetized with 10% chloral hydrate by intraperitoneal injection. Hereafter, 100 μl of MMB-SiO_2-tPA at the equivalent concentration of tPA (10 μg ml^{-1}) was administered. Then, a magnet was placed in the middle of the mice tail. Ultrasound with different intensities (0.2 and 0.5 bar) was applied, respectively. Last, 5 cm of the distal tail was removed from the mice for histological analysis.

Statistical analysis

All data were expressed as means ± SD. Inter- and intragroup comparisons and analysis in each experiment were performed by

unpaired Student's *t* test and one-way analysis of variance (ANOVA) using the SPSS software. Probability (*P*) values of <0.05 were considered statistically significant.

SUPPLEMENTARY MATERIALS

Supplementary material for this article is available at http://advances.sciencemag.org/cgi/content/full/6/31/eaaz8204/DC1

View/request a protocol for this paper from *Bio-protocol*.

REFERENCES AND NOTES

1. B. Furie, B. C. Furie, Mechanisms of thrombus formation. *N. Engl. J. Med.* **359**, 938–949 (2008).
2. N. Mackman, Triggers, targets and treatments for thrombosis. *Nature* **451**, 914–918 (2008).
3. World Health Organization, *Global Health Estimates 2016: Disease burden by cause, age, sex, by country and by region, 2000–2016* (World Healh Organization, 2018); https://who.int/healthinfo/global_burden_disease/estimates/en/index1.html.
4. S. T. Gunawan, K. Kempe, T. Bonnard, J. Cui, K. Alt, L. S. Law, X. Wang, E. Westein, G. K. Such, K. Peter, C. E. Hagemeyer, F. Caruso, Multifunctional thrombin-activatable polymer capsules for specific targeting to activated platelets. *Adv. Mater.* **27**, 5153–5157 (2015).
5. L. Derex, N. Nighoghossian, Thrombolysis, stroke-unit admission and early rehabilitation in elderly patients. *Nat. Rev. Neurol.* **5**, 506–511 (2009).
6. C. A. Molina, J. Montaner, J. F. Arenillas, M. Ribo, M. Rubiera, J. Alvarez-Sabin, Differential pattern of tissue plasminogen activator-induced proximal middle cerebral artery recanalization among stroke subtypes. *Stroke* **35**, 486–490 (2004).
7. V. J. Marder, V. Novokhatny, Direct fibrinolytic agents: Biochemical attributes, preclinical foundation and clinical potential. *J. Thromb. Haemostasis* **8**, 433–444 (2010).
8. J. Xu, X. Wang, H. Yin, X. Cao, Q. Hu, W. Lv, Q. Xu, Z. Gu, H. Xin, Sequentially site-specific delivery of thrombolytics and neuroprotectant for enhanced treatment of ischemic stroke. *ACS Nano* **13**, 8577–8588 (2019).
9. C. Li, H. Du, A. Yang, S. Jiang, Z. Li, D. Li, J. L. Brash, H. Chen, Thrombosis-responsive thrombolytic coating based on thrombin-degradable tissue plasminogen activator (t-PA) nanocapsules. *Adv. Funct. Mater.* **27**, 1703934 (2017).
10. E. Voros, M. Cho, M. Ramirez, A. L. Palange, E. De Rosa, J. Key, Z. Garami, A. B. Lumsden, P. Decuzzi, TPA immobilization on iron oxide nanocubes and localized magnetic hyperthermia accelerate blood clot lysis. *Adv. Funct. Mater.* **25**, 1709–1718 (2015).
11. Y. Zhong, Y. Zhang, J. Xu, J. Zhou, J. Liu, M. Ye, L. Zhang, B. Qiao, Z.-G. Wang, H.-T. Ran, D. Guo, Low-intensity focused ultrasound-responsive phase-transitional nanoparticles for thrombolysis without vascular damage: A synergistic nonpharmaceutical strategy. *ACS Nano* **13**, 3387–3403 (2019).
12. N. Korin, M. Kanapathipillai, B. D. Matthews, M. Crescente, A. Brill, T. Mammoto, K. Ghosh, S. Jurek, S. A. Bencherif, D. Bhatta, A. U. Coskun, C. L. Feldman, D. D. Wagner, D. E. Ingber, Shear-activated nanotherapeutics for drug targeting to obstructed blood vessels. *Science* **337**, 738–742 (2012).
13. R. Cheng, W. Huang, L. Huang, B. Yang, L. Mao, K. Jin, Q. ZhuGe, Y. Zhao, Acceleration of tissue plasminogen activator-mediated thrombolysis by magnetically powered nanomotors. *ACS Nano* **8**, 7746–7754 (2014).
14. S. T. Laing, M. Moody, B. Smulevitz, H. Kim, P. Kee, S. Huang, C. K. Holland, D. D. McPherson, Ultrasound-enhanced thrombolytic effect of tissue plasminogen activator-loaded echogenic liposomes in an in vivo rabbit aorta thrombus model—Brief report. *Arterioscler. Thromb. Vasc. Biol.* **31**, 1357–1359 (2011).
15. S. T. Laing, M. R. Moody, H. Kim, B. Smulevitz, S.-L. Huang, C. K. Holland, D. D. McPherson, M. E. Klegerman, Thrombolytic efficacy of tissue plasminogen activator-loaded echogenic liposomes in a rabbit thrombus model. *Thromb. Res.* **130**, 629–635 (2012).
16. C. F. Greineder, M. D. Howard, R. Carnemolla, D. B. Cines, V. R. Muzykantov, Advanced drug delivery systems for antithrombotic agents. *Blood* **122**, 1565–1575 (2013).
17. T. O. Tasci, D. Disharoon, R. M. Schoeman, K. Rana, P. S. Herson, D. W. M. Marr, K. B. Neeves, Enhanced fibrinolysis with magnetically powered colloidal microwheels. *Small* **13**, 1700954 (2017).
18. C. L. Pawlowski, W. Li, M. Sun, K. Ravichandran, D. Hickman, C. Kos, G. Kaur, A. Sen Gupta, Platelet microparticle-inspired clot-responsive nanomedicine for targeted fibrinolysis. *Biomaterials* **128**, 94–108 (2017).
19. J. Hu, S. Huang, L. Zhu, W. Huang, Y. Zhao, K. Jin, Q. ZhuGe, Tissue plasminogen activator-porous magnetic microrods for targeted thrombolytic therapy after ischemic stroke. *ACS Appl. Mater. Interfaces* **10**, 32988–32997 (2018).
20. Y. Gao, C. U. Chan, Q. Gu, X. Lin, W. Zhang, D. C. L. Yeo, A. M. Alsema, M. Arora, M. S. K. Chong, P. Shi, C.-D. Ohl, C. Xu, Controlled nanoparticle release from stable magnetic microbubble oscillations. *NPG Asia Mater.* **8**, e260 (2016).
21. A. Alzaraa, G. Gravante, W. Y. Chung, D. Al-Leswas, M. Bruno, A. R. Dennison, D. M. Lloyd, Targeted microbubbles in the experimental and clinical setting. *Am. J. Surg.* **204**, 355–366 (2012).
22. Z. Tang, D. Li, X. Wang, H. Gong, Y. Luan, Z. Liu, J. L. Brash, H. Chen, A t-PA/nanoparticle conjugate with fully retained enzymatic activity and prolonged circulation time. *J. Mater. Chem. B* **3**, 977–982 (2015).
23. J. R. Lindner, Microbubbles in medical imaging: Current applications and future directions. *Nat. Rev. Drug Discov.* **3**, 527–532 (2004).
24. Y. Luan, G. Lajoinie, E. Gelderblom, I. Skachkov, A. F. W. van der Steen, H. J. Vos, M. Versluis, N. De Jong, Lipid shedding from single oscillating microbubbles. *Ultrasound Med. Biol.* **40**, 1834–1846 (2014).
25. H. Chen, W. Kreider, A. A. Brayman, M. R. Bailey, T. J. Matula, Blood vessel deformations on microsecond time scales by ultrasonic cavitation. *Phys. Rev. Lett.* **106**, 034301 (2011).
26. P. Prentice, A. Cuschieri, K. Dholakia, M. Prausnitz, P. Campbell, Membrane disruption by optically controlled microbubble cavitation. *Nat. Phys.* **1**, 107–110 (2005).
27. D. Collen, H. R. Lijnen, Thrombolytic agents. *Thromb. Haemost.* **93**, 627–630 (2005).
28. J. Xu, Y. Zhang, J. Xu, G. Liu, C. Di, X. Zhao, X. Li, Y. Li, N. Pang, C. Yang, Y. Li, B. Li, Z. Lu, M. Wang, K. Dai, R. Yan, S. Li, G. Nie, Engineered nanoplatelets for targeted delivery of plasminogen activators to reverse thrombus in multiple mouse thrombosis models. *Adv. Mater.* **32**, e1905145 (2020).
29. K. Y. Lin, J. H. Lo, N. Consul, G. A. Kwong, S. N. Bhatia, Self-titrating anticoagulant nanocomplexes that restore homeostatic regulation of the coagulation cascade. *ACS Nano* **8**, 8776–8785 (2014).
30. A. Nacu, C. E. Kvistad, H. Naess, H. Øygarden, N. Logallo, J. Assmus, U. Waje-Andreassen, K. D. Kurz, G. Neckelmann, L. Thomassen, NOR-SASS (Norwegian Sonothrombolysis in Acute Stroke Study): Randomized controlled contrast-enhanced sonothrombolysis in an unselected acute ischemic stroke population. *Stroke* **48**, 335–341 (2017).
31. H. Chen, A. A. Brayman, M. R. Bailey, T. J. Matula, Blood vessel rupture by cavitation. *Urol. Res.* **38**, 321–326 (2010).
32. A. V. Alexandrov, C. A. Molina, J. C. Grotta, Z. Garami, S. R. Ford, J. Alvarez-Sabin, J. Montaner, M. Saqqur, A. M. Demchuk, L. A. Moyé, M. D. Hill, A. W. Wojner; CLOTBUST Investigators, Ultrasound-enhanced systemic thrombolysis for acute ischemic stroke. *N. Engl. J. Med.* **351**, 2170–2178 (2004).
33. S. Absar, K. Nahar, Y. M. Kwon, F. Ahsan, Thrombus-targeted nanocarrier attenuates bleeding complications associated with conventional thrombolytic therapy. *Pharm. Res.* **30**, 1663–1676 (2013).
34. J. Zhou, D. Guo, Y. Zhang, W. Wu, H. Ran, Z. Wang, Construction and evaluation of Fe_3O_4-based PLGA nanoparticles carrying rtPA used in the detection of thrombosis and in targeted thrombolysis. *ACS Appl. Mater. Interfaces* **6**, 5566–5576 (2014).
35. T. Bonnard, Z. Tennant, B. Niego, R. Kanojia, K. Alt, S. Jagdale, L. S. Law, S. Rigby, R. L. Medcalf, K. Peter, C. E. Hagemeyer, Novel thrombolytic drug based on thrombin cleavable microplasminogen coupled to a single-chain antibody specific for activated GPIIb/IIIa. *J. Am. Heart Assoc.* **6**, e004535 (2017).
36. Q. Hu, C. Qian, W. Sun, J. Wang, Z. Chen, H. N. Bomba, H. Xin, Q. Shen, Z. Gu, Engineered nanoplatelets for enhanced treatment of multiple myeloma and thrombus. *Adv. Mater.* **28**, 9573–9580 (2016).
37. M. Colasuonno, A. L. Palange, R. Aid, M. Ferreira, H. Mollica, R. Palomba, M. Emdin, M. Del Sette, C. Chauvierre, D. Letourneur, P. Decuzzi, Erythrocyte-inspired discoidal polymeric nanoconstructs carrying tissue plasminogen activator for the enhanced lysis of blood clots. *ACS Nano* **12**, 12224–12237 (2018).
38. J. Shao, M. Abdelghani, G. Shen, S. Cao, D. S. Williams, J. C. M. van Hest, Erythrocyte membrane modified janus polymeric motors for thrombus therapy. *ACS Nano* **12**, 4877–4885 (2018).
39. J.-C. Murciano, S. Medinilla, D. Eslin, E. Atochina, D. B. Cines, V. R. Muzykantov, Prophylactic fibrinolysis through selective dissolution of nascent clots by tPA-carrying erythrocytes. *Nat. Biotechnol.* **21**, 891–896 (2003).
40. J. N. Marsh, G. Hu, M. J. Scott, H. Zhang, M. J. Goette, P. J. Gaffney, S. D. Caruthers, S. A. Wickline, D. Abendschein, G. M. Lanza, A fibrin-specific thrombolytic nanomedicine approach to acute ischemic stroke. *Nanomedicine* **6**, 605–615 (2011).
41. X. Wang, C. Wei, M. Liu, T. Yang, W. Zhou, Y. Liu, K. Hong, S. Wang, H. Xin, X. Ding, Near-infrared triggered release of uPA from nanospheres for localized hyperthermia-enhanced thrombolysis. *Adv. Funct. Mater.* **27**, 1701824 (2017).

Acknowledgments

Funding: This work was supported by the National Key Research and Development Program of China (2017YFA0205302), the National Natural Science Foundation of China (81601608, 21475064), the Natural Science Foundation of Jiangsu Province of China (BK20160919), the Key Research and Development Program of Jiangsu (BE2018732), the Natural Science Key Fund for Colleges and Universities in Jiangsu Province (17KJA430011), and NUPTSF (NY216024). **Author contributions:** Y.G., S.W., and L.W. designed the study. S.W. carried out

microbubble synthesis, characterization, and all in vitro assays. S.W., X.G., W.X., L.R., and H.X. performed the ex vivo and animal experiments. Y.L. and F.Y. helped with the ultrasound imaging experiments. C.X. helped and gave valuable suggestions for the animal experiments. Y.G., S.W., C.X., and L.W. wrote the manuscript. All authors discussed the results and commented on the manuscript. **Competing interests:** The authors declare that they have no competing interests. **Data and materials availability:** All data needed to evaluate the conclusions in the paper are present in the paper and/or the Supplementary Materials. Additional data related to this paper may be requested from the authors.

Submitted 15 October 2019
Accepted 12 June 2020
Published 29 July 2020
10.1126/sciadv.aaz8204

Citation: S. Wang, X. Guo, W. Xiu, Y. Liu, L. Ren, H. Xiao, F. Yang, Y. Gao, C. Xu, L. Wang, Accelerating thrombolysis using a precision and clot-penetrating drug delivery strategy by nanoparticle-shelled microbubbles. *Sci. Adv.* **6**, eaaz8204 (2020).